Investigating β-decay properties of spherical nuclei along the possible r-process path

Dong-Liang Fang,[1,2] B. Alex Brown,[1,2,3] and Toshio Suzuki[4,5]

[1]*National Superconducting Cyclotron Laboratory, Michigan State University, East Lansing, Michigan 48824, USA*

[2]*Joint Institute for Nuclear and Astrophysics, Michigan State University, East Lansing, Michigan 48824, USA*

[3]*Department of Physics and Astronomy, Michigan State University, East Lansing, Michigan 48824, USA*

[4]*Department of Physics, College of Humanities and Sciences, Nihon University, Sakurajosui 3-25-40, Setagaya-ku, Tokyo 156-8550, Japan*

[5]*National Astronomical Observatory of Japan, Mitaka, Tokyo 181-8588, Japan*

(Received 21 June 2013; revised manuscript received 6 August 2013; published 3 September 2013)

The spherical quasiparticle random-phase approximation method is used for calculations of the β-decay properties of neutron-rich nuclei in the region near the neutron magic numbers $N = 82$ and $N = 126$ which are important for determination of the r-process path. Our calculations differ from previous works by the use of realistic forces for the proton-neutron interaction. Both allowed and first-forbidden β decays are included. Detailed comparisons with the experimental measurements and the previous shell-model calculations are performed. The results for half-lives and β-delayed neutron emission probabilities will serve as input for r-process nucleosynthesis simulations.

DOI: 10.1103/PhysRevC.88.034304 PACS number(s): 21.10.Tg, 21.60.Jz, 23.40.Hc, 26.30.Hj

I. INTRODUCTION

The synthesis of the heavy elements in the universe is one of the most important and interesting topics in modern physics. Different processes and astrophysical events are involved in understanding the measured isotopic abundances. One kind of process is the so-called rapid-neutron capture process (r-process), which gives rise to heavy elements beyond iron in our solar system [1,2]. The site of this process is still not clear. One of the popular ideas is the high-entropy wind of core collapse Type II supernovae [2–4]. The obstacles to the simulation of the r-process are twofold: (1) The unclear site gives uncertainties to the astrophysical environmental parameters which are crucial for the initial conditions of the simulations of r-process evolution, such as the initial neutron richness and the temperature [4]. (2) Most of the nuclei involved in the evolution are exotic neutron-rich ones which are currently out of the reach of experiments, so their reaction and decay rates are still uncertain. For the r-process the nuclei are very neutron rich and some are near the neutron drip line. The general pattern of solar element abundance shows peaked distributions around $A \sim 130$ and $A \sim 190$. Surveys [2] show that in order to produce these two heavy-element peaks, the properties of nuclei around $A \sim 130$ and 190 are important, especially those near the proton or neutron magic numbers.

The nuclear chart can be divided into regions near the magic numbers where the low-lying states are best described in a spherical basis and regions in between the magic numbers where they are best described in a deformed basis. The quasiparticle random-phase approximation (QRPA) method has been developed for each of these. There is a transitional region that, at present, must be interpolated in terms of the spherical and deformed limits. In a previous paper we focused on the deformed region of nuclei centered on $Z = 46$ and $N = 66$ [5]. In this work we will focus on the heavy spherical nuclei near the magic numbers. In these regions, some shell-model calculations can be performed with a truncated model space. Early calculations only included Gamow-Teller (GT) decay [6,7], but recent calculations [8–10] have also included first-forbidden (FF) decays, which turn out to be important for the $N = 126$ isotones [8]. QRPA methods have previously been used; these include the QRPA method with separable forces in [11–13], the self-consistent QRPA from density functional theory [14], and the continuum QRPA [15,16]. As an improved alternative, we propose the proton-neutron quasiparticle random-phase approximation method with realistic forces as introduced in [17,18]. The advantage of this method is that with the G matrix obtained from the Bethe equations with realistic potentials fitted from the nucleon-nucleon scattering data, one can obtain the full spectrum for the ground as well as excited states of the odd-odd daughter nuclei. The full spectrum provides an exact treatment for the excitation energies which are missing in most other QRPA methods. The inclusion of states with more spin-parities also means that we can deal with the negative-parity FF transitions which are missing in some calculations [11,12].

This article is arranged as follows. In the next section the QRPA method and its application to allowed and forbidden β decay is outlined. The choice of model parameters is discussed in Sec. III. The results are presented in Sec. IV in comparison with experiment and to previous calculations. Section V presents the conclusions.

II. FORMALISM AND METHOD

In this work, we will calculate both the allowed GT and FF β decays for proton-neutron even-even and odd-even nuclear isotones near $N = 82$ and $N = 126$. The half-lives for these decays can be expressed generally as

$$T_{1/2} = \frac{\ln 2}{\Gamma}. \tag{1}$$

Here $\Gamma = \sum_i \Gamma_i$ is the total decay width and is a sum over all the possible decay widths from the ground state of the initial parent nucleus to different states of the final daughter nucleus with the specific selection rules. For GT decay, the width can be expressed as

$$\Gamma_i^{\mathrm{GT}} = (f_0/K_0) g_A^2 B_i(\mathrm{GT}^-). \tag{2}$$

The term f_0 is the dimensionless phase-space factor depending on the β-decay Q_β value [19], while K_0 is a combinations

of constants defined as $K_0 = \frac{2\pi^3\hbar^7}{m_e^5c^4}$. The GT strength $B(\mathrm{GT}^-)$ can be expressed in terms of the reduced matrix element for spherical nuclei $B(\mathrm{GT}^-) = |M_i(\mathrm{GT}^-)|^2/(2J+1)$, where J is the spin of the parent nucleus. A frequently used quantity here is the log ft value, which is defined here as $\log ft = \log[\frac{C}{g_A^2 B(\mathrm{GT}^-)}]$ with $C = \ln 2K_0 = 6170$.

For FF decay, the expression is more complicated, as in [19]

$$\Gamma_i^{\mathrm{FF}} = \frac{f_i}{8896}\ (\mathrm{s}^{-1}), \tag{3}$$

with

$$f_i = \int_1^{\omega} \mathcal{C}(\omega)F(Z,\omega)p\omega(\omega_0-\omega)^2 d\omega, \tag{4}$$

and with $\mathcal{C}(\omega)$ defined as

$$\mathcal{C}(\omega) = k + ka\omega + kb/\omega + kc\omega^2. \tag{5}$$

$\omega = E_e/m_ec^2$ is the electron energy in units of the electron mass, $F(Z,\omega)$ is the Fermi function as expressed in [19], and k, ka, kb, and kc are the nuclear matrix elements depending on the nuclear structure. The detailed expressions for these matrix elements are given in Eq. (8) in Ref. [10] and Eqs. (3)–(5) in Ref. [8]. The log ft values in this case are defined as $\log ft = \log(f_0C/\Gamma_i^{\mathrm{FF}})$, where f_0 is the phase-space factor for GT decay.

In this work, for the matrix element calculations, we adopt the proton-neutron quasiparticle random-phase approximation (pn-QRPA) method. The quasiparticle concept starts with nuclear pairing. The most common description of pairing in nuclear physics is the BCS formalism. Under the BCS formalism, one can define the quasiparticle operator $\alpha_\tau = u_\tau c_\tau + v_\tau \tilde{c}_\tau^\dagger$, where u_τ and v_τ are the BCS coefficients solved from BCS equations and $c_\tau^\dagger$ is the single-particle creation operator. With the quasiparticle operators, one can define the QRPA phonons as [17]

$$Q_{J^\pi M}^{m\dagger} = \sum_{pn} X_{pn}^m A_{pn,J^\pi M}^\dagger - Y_{pn}^m \tilde{A}_{pn,J^\pi M}. \tag{6}$$

Here the two quasiparticle operators are defined as $A_{pn,J^\pi M}^\dagger \equiv [\alpha_p^\dagger \alpha_n^\dagger]_{J^\pi M}$, with p and n being proton and neutron, respectively. The coefficients X's and Y's here are the forward and backward amplitudes, respectively. They can be derived from the solutions of the QRPA equations [17,18]:

$$\begin{pmatrix} A & B \\ B & A \end{pmatrix}\begin{pmatrix} X \\ Y \end{pmatrix} = \omega \begin{pmatrix} 1 & 0 \\ 0 & -1 \end{pmatrix}\begin{pmatrix} X \\ Y \end{pmatrix}. \tag{7}$$

Here, $A_{pn,p'n'} = [A_{pn}, [H, A_{p'n'}^\dagger]]$ and $B_{pn,p'n'} = [A_{pn}^\dagger, [H, \tilde{A}_{p'n'}^\dagger]]$. The Hamiltonian and the detailed expressions for A and B with realistic interactions have been presented in Ref. [17]. In this scenario, the different excited states are defined as $|J^\pi M; m\rangle \equiv Q_{J^\pi M}^{m\dagger}|0\rangle$ with the QRPA phonon $Q_{J^\pi M}^m$ acted on an even-even vacuum $|0\rangle$.

For decays of even-even nuclei we choose the BCS vacuum as the ground state:

$$|0\rangle_i = |QRPA\rangle \approx |BCS\rangle, \tag{8}$$

while the final states in the odd-odd nuclei are the pn-QRPA excited states as defined by

$$|m\rangle_f = Q_{J^\pi}^{m\dagger}|0\rangle. \tag{9}$$

The solved QRPA energies are to some extent relative to the parent nuclei and cannot be used directly as the excitation energies. Since the ground states of the daughter nuclei should be the ones which also have the lowest energies relative to the parents, we set the energies of the states which have the lowest QRPA energies to be ground states of the daughter with zero excitation energies. The energies of all the excited states are then $E_m = \omega_{m,J^\pi} - \omega_{g.s.}$, where the ω_m refer to the eigenvalues of the mth state from the QRPA solutions in the spherical systems while $\omega_{g.s.}$ is the smallest eigenvalues of the solutions. The effective Q_β values for each state are $Q_m = Q - E_m$, where Q_β is the mass difference between the two ground states of parent and daughter nuclei.

To obtain the lifetime, besides the Q_β values, one also needs the matrix elements in Eqs. (2)–(5), for even-even to odd-odd decay. These can be expressed in our formalism as

$$\langle J^\pi m\big|\big|\tau^+ O_I^{K^\pi}\big|\big|0\rangle_i = \delta_{J,K}\sum_{pn}\langle p\big|\big|\tau^+ O_I^{K\pi}\big|\big|n\rangle \times \left(X^{J^\pi,m}u_p v_n + Y^{J^\pi,m}v_p u_n\right). \tag{10}$$

Here the $O_I^{K^\pi}$ is the nuclear transition operator for β decay. The reduced matrix elements from the Wigner-Eckart theorem are independent of M (the projection of total angular momentum onto the z axis). For the allowed decay, $O_{GT}^{1^+} = \sigma$ with the selection rule $\Delta J = K = 1$ and $\Delta\pi = 1$, while for first-forbidden decay, the expressions for the operators are more complicated (with detailed forms given in [8]) with the selection rules $\Delta J = K = 0, 1, 2$ and $\Delta\pi = -1$.

For decays of odd-even nuclei, one has an unpaired nucleon; the simplest scenario is that given in Ref. [11]. One quasiparticle or one quasiparticle plus one QRPA phonon acts on the BCS vacuum (the spectator mode in [11]). In Ref. [11], for the single-particle excitations, the correction from the coupling between the single quasiparticle and the QRPA phonon was taken into consideration with the assumption of the weak-coupling limit. In our calculation we find that this correction gives only small changes. Since it takes a much longer time for the calculation, we neglect this effect in the present calculation.

We have two kinds of states for odd-even nuclei. First, we have the single-particle state as given by

$$|\tau\rangle_i = \alpha_{\tau_i}^\dagger|0\rangle.$$

Here τ can be either a proton or a neutron. The ground states of the parent nuclei are chosen to be the ones with the lowest quasiparticle energies, and this also holds for the even-odd daughter nuclei. For all the other single-quasiparticle excitations, the relative excitation energies to the ground state are $E_i = E_{\tau,i} - E_0$.

Another kind of state for the daughter nuclei is the quasiparticle plus phonon state mentioned above without the possible mixing between them:

$$|\omega_{K^\pi M',m},\tau';J^\pi M\rangle = C_{K,M';j_{\tau'}m_{\tau'}}^{J^\pi,M} Q_{K^\pi,m}^\dagger \alpha_{\tau'}^\dagger|0\rangle. \tag{11}$$

The energies of such states are determined as follows. If we compare such states with the odd-odd nuclei, the only difference is the spectator single quasiparticle; the difference of excitation energies in the two systems is simply equivalent to the difference of the Q_β values in these two systems (corresponding to the difference of the ground states), which gives $E_{m,0} = Q_{oe} - Q_{ee} + \omega_m - \omega_{g.s.}$.

The matrix elements for β decay of odd-even nuclei to these two different kinds of final states can be written as

$$\langle n_i || \tau^+ O_I^{K^\pi} || p_0 \rangle = u_{p_0} u_{n_i} \langle p_0 || \sigma || n_i \rangle$$

and

$$\begin{aligned} &\langle \omega_{K^\pi,m},\, p'; J^\pi M || \tau^+ O_I^{K^\pi} || p_0 \rangle \\ &= -\sqrt{(2J+1)(2j_{p_0}+1)} \\ &\quad \times \delta_{p_0,p'} \begin{Bmatrix} K & J & j_{p_0} \\ j_{p_0} & 0 & K \end{Bmatrix} \langle \omega_{K^\pi,m} || \tau^+ O_I^{K^\pi} || 0 \rangle \end{aligned} \tag{12}$$

with $O_I^{K\pi}$ of the same form as for the even-even case.

With these derived excitation energies and matrix elements, we can calculate the β-decay properties with the results presented in the next sections.

III. CHOICE OF PARAMETERS

In this work, we are interested in nuclei near or on the neutron magic numbers 82 and 126. We chose the isotonic chains with $N = 80$, 82, and 84 and $N = 124$, 126, and 128. Many of these nuclei are on the r-process path and their decay properties are important for the r-process path that determines the final element productions near the peaks.

For single-particle (SP) energies, we adopt here those derived from solution of the Hartree-Fock equations with the SkX Skyrme interaction [20]. For the unbound positive-energy states, we make an approximate extrapolation for their discrete energies. We choose the QRPA model space as follows. We include all the SP levels with energies up to 5 MeV for neutrons and protons. For the pairing part, the BCS equations are solved with constant pairing gaps obtained from the symmetric five-term formula [26], where the pairing gaps are derived from the odd and even mass differences. The obtained BCS coefficients and quasiparticle energies are then used as inputs for the QRPA equations as described above. For odd-even nuclei, the BCS solutions are especially important for nuclei with small Q_β values, since they determine which single-particle transitions are important for the lowest energies.

For the residual interactions, we adopt the Brückner G matrix derived from the CD-Bonn potential [21]. Two different parts of the interaction are included, namely, the particle-hole channel and particle-particle channel interactions. The two-body matrix elements are calculated with harmonic-oscillator radial wave functions. Renormalization of the matrix elements has been introduced to empirically take into consideration the effect of the truncations of the model space over the infinite Hilbert space into those orbitals in the model space. For simplicity, two overall factors are introduced, namely, g_{ph} (for the particle-hole channel) and g_{pp} (for the particle-particle channel). The parameter g_{ph} mainly determines the position of the giant Gamow-Teller resonance (GTR). Since there is no coupling between the GTR and the low-lying states the GT β decay to low-lying states is not affected by the value of g_{ph}. Although for large Q_β values some of the decay could go to the lower part of the GTR, this contributes little to the total decay width due to their higher energies, but it could be important for the β-delayed neutron decay branches. A value of $g_{ph} = 1$, which reproduces the experimental energy, is adopted here.

TABLE I. The experimental 1^+ energies and corresponding log ft values of the largest decay branch for different even-even Cd isotopes and also the corresponding half-lives. A comparison between the experimental measurements and theoretical calculations has been made with quenching factors $q \equiv g_A/g_{A0} = 0.4$. Here $g_{A0} = 1.26$ is the axial-vector-coupling constant for free neutrons.

		Experiment [29,31]			Calculation	$q = 0.4$	
	N	E_{1^+}	log ft	$t_{1/2}$ (s)	E_{1^+}	log ft	$t_{1/2}$ (s)
^{118}Cd	70	0	3.91	3018(12)	0	3.84	2484
^{120}Cd	72	0	4.10	50.80(21)	0	3.90	32.2
^{122}Cd	74	0	3.95	5.24(3)	0.04	3.97	4.76
^{124}Cd	76			1.25(2)	0.40	4.02	1.79
^{126}Cd	78			0.515(17)	0.70	4.09	0.67
^{128}Cd	80	1.17	4.17	0.28(4)	1.02	4.11	0.25
^{130}Cd	82	2.12	4.10	0.162(7)	1.18	4.14	0.12
^{132}Cd	84			0.097(10)	4.62	4.27	0.14

The other parameter, g_{pp}, affects the energies of low-lying excited states and the GT matrix elements to these states. The 1^+ excitation energies are sensitive to the value of g_{pp}. For nuclei near $N = 82$, g_{pp} values around 0.8 best reproduce details of the energy levels (see Table I). For nuclei near $N = 126$ there are limited data on the final-state energies (especially for 1^+). As we shall show later, the quenching values we chose seem to agree with the experimental results, but we find that $g_{pp} = 1.0$ better reproduces the half-lives. These parameters are obtained for the even-even nuclei, and for consistency the same values are used in odd-mass nuclei.

In this work, we also introduce a quenching effect since our calculations show an overall underestimation of half-lives compared with the experimental measurements for cases where there is good agreement for excitation energies. This quenching of the QRPA calculations for spherical nuclei may have two origins. The GT strengths obtained with shell-model calculations in the sd shell [22] and pf shell [23] are systematically larger than experimental values by about a factor of 2. The "quenching" of experiment relative to theory by about a factor of 0.5 is consistent with results obtained by second-order perturbation theory corrections that take into account the excitation of nucleons outside of these model spaces [24,25].

Second, in spherical QRPA calculations, only one-phonon excitations have been taken into account, while shell-model calculations show that there exists mixing between the single- and multiphonon states. Two kinds of mixing outside of our model could be present: the low-lying part mixes with the GTR, which shifts strength to higher energy, and the charge-conserving one-particle–one-hole excitations couple with charge-exchange GT excitations, which spreads the GT

strength and shifts some of the strength to higher energies. We determine the quenching empirically by comparing the calculated log ft values and half-lives with the experimental ones for the Cd isotopes. The results are shown in Table I. The log ft values are for individual final states, while the half-lives take into account the decay to all final states (GT being the dominate decay mode). A choice of $g_A/g_{A0} \approx 0.4$ generally reproduces the half-lives. The largest difference comes from ^{130}Cd because we predict a smaller excitation energy compared to experiment. From this comparison, we adopt the value of $g_A/g_{A0} = 0.4$ for the GT calculation as an optimal choice in our calculation for both $N = 82$ and $N = 126$ regions.

Compared to the simple σ operator for GT decays, the FF operators are more complicated with several different spin-parity combinations. As was shown in [32], the tensor part of the 0^+ to 0^- FF operator is enhanced due to mesonic-exchange currents. As in Ref. [10] we use an enhancement factor of $\epsilon = 2$. In general, we could use different quenchings for the other types of FF operators as was done for the shell-model calculations of Ref. [10]. However, this is quite complicated and, even with least-square fits in Table I of Ref. [10], we still see some large deviations, We cannot simply use the same quenching adopted in the shell-model approach since the origins of quenching for the shell model and the QRPA are different. For the shell model it comes from the model-space truncation (with a rather small model space compared with the QRPA calculation), while for QRPA, it is from the configuration-space truncation (since only one-phonon excitations have been taken into account in the QRPA). In this sense, different quenching schemes should be used. For simplicity, we use an overall quenching factor for all the FF operators and we vary this value to find the best agreement to a rather limited set of data.

The quenching factors $g_A/g_{A0} = 0.5$ and $g_V/g_{V0} = 0.5$ for FF transitions are obtained in this way by comparing the theory to experiment for some relatively strong FF transitions to low-lying states. In Table II, the comparison between experiment and theory with and without the chosen quenching factors for the decay of Te and Xe isotopes is shown. Without quenching, there is a general underestimation of about 0.6 in the log ft values. When we use the above quenching, for most decay branches, this deviation reduces to less than 0.3. The same quenching factors are used in the $N = 126$ region.

For the odd-mass nuclei, the same parameter sets (g_{pp} and g_A) are adopted. The results for some FF branch ratios are shown in Table III. The deviation of the log ft values are generally larger than in the even-even case. We see reasonable agreement for ^{139}Cs and ^{203}Au. The ^{207}Tl to ^{207}Pb decay is particularly simple. When experimental single-particle energies are used the transition is dominated by the $3s_{1/2}$ to $2p_{1/2}$ contribution and we obtain log $ft = 5.11$ (with quenching) compared to the experimental value of 5.02. In general, our QRPA approach is not very good for cases with one or two nucleons removed from the doubly magic nuclei where the pairing is weak and the BCS solution sometimes overestimates the pairing effect. Also transitions to a few low-lying states are sensitive to the precise value of the single-particle energies. (The SkX single-particle energies differ from experiment by up to 0.5 MeV; see Fig. 4 in [20].)

TABLE II. Decay schemes for three even-even isotopes near ^{132}Sn. For understanding the FF decays, we show the spin-parties, excitation energies, and log ft values for several important FF decay branches. For the two theoretical log ft values, the one without a subscript uses the quenching factors $g_A = 0.5g_{A0}$ and $g_V = 0.5g_{V0}$ while the subscript u means no quenching has been taken into account. For both cases, an enhancement factor $\epsilon = 2$ for the tensor part of 0^- transitions is adopted [32].

	Experiment [29]				Theory			
	J_i^π	J_f^π	E_{ex}	log ft	log ft_q	log ft_u	J_f^π	E_{ex}
	0^+	$1^-, 0^-$	0.080	6.14	6.15	5.55	0^-	0
^{140}Xe		$(0, 1^-)$	0.515	6.82	6.58	5.98	1^-	0.127
		$0^{(-)}, 1^{(-)}$	0.653	5.98	5.90	5.29	1^-	0.586
		$(1, 2^-)$	0.800	≈7.1	7.36	6.22	2^-	0.370
		$1^{(-)}$	0.966	6.77	6.56	5.95	1^-	1.350
	0^+	2^-	0.011	>8.5	7.62	7.01	2^-	0.041
^{138}Xe		$(1)^-$	0.016	7.2	7.01	6.41	1^-	0.111
		$1^-, 2^-$	0.258	7.32	7.42	6.82	2^-	0.349
		1^-	0.412	6.79	6.29	5.68	1^-	0.563
		$0^-, 1^-$	0.450	6.59	6.52	5.92	0^-	0
	0^+	(1^-)	0	>6.7	6.72	6.16	1^-	0.169
^{136}Te		$(0^-, 1, 2^-)$	0.222	7.23	6.79	6.19	2^-	0.540
		$(0^-, 1)$	0.334	6.27	6.00	5.39	1^-	0.749
		$(0^-, 1)$	0.631	6.28	6.37	5.77	1^-	0
		$(0^-, 1, 2^-)$	0.738	7.57	7.70	7.09	2^-	0.194

For global parameters such as Q_β values and neutron separation energies, we use the experimental values if they are available; otherwise, we use the masses predicted by some phenomenological mass models. For comparisons, we used two mass models here: the finite-range droplet mass (FRDM) model [12] and the Hartree-Fock-Boglyubov model HFB21 [28].

TABLE III. The decay schemes for several odd-even isotopes for both the experimental measurements and the theoretical calculations. We show the spin-parities, excitation energies, and log ft values for several decay branches which have the largest branch ratios. The parameters adopted here are $g_{pp} = 1$ and $g_A(g_V) = 0.5g_{A0}(g_{V0})$.

		Experiment [29]			Theory		
	J_i^π	J_f^π	E_{ex}	log ft	J_f^π	E_{ex}	log ft
	$7/2^+$	$7/2^-$	0.051	6.88	$7/2^-$	0	6.63
^{139}Cs		$9/2^-$	1.283	7.4	$9/2^-$	0.824	6.77
		$5/2^-, 7/2^-$	2.349	7.3	$7/2^-$	3.308	6.66
	$3/2^+$	$3/2^-$	0.051	5.63	$3/2^-$	0.333	5.18
^{203}Au		$3/2^-$	0.225	6.61	$1/2^-$	0	7.16
		$5/2^-$	0	5.19	$5/2^-$	0.418	5.11
	$3/2^+$	$1/2^-$	0	5.79	$1/2^-$	0	7.06
^{205}Au		$3/2^-$	0.468	6.43	$3/2^-$	0.336	5.15
		$5/2^-$	0.379	6.37	$3/2^-$	0.761	5.07
	$1/2^+$	$1/2^-$	0.379	5.11	$1/2^-$	0	5.02
^{207}Tl[a]		$3/2^-$	0.898	6.16	$3/2^-$	0.624	6.56

[a]For this nucleus, we used the BCS coefficients extracted from the shell model to replace the solved BCS coefficients, which are poorly reproduced near doubly magic nuclei.

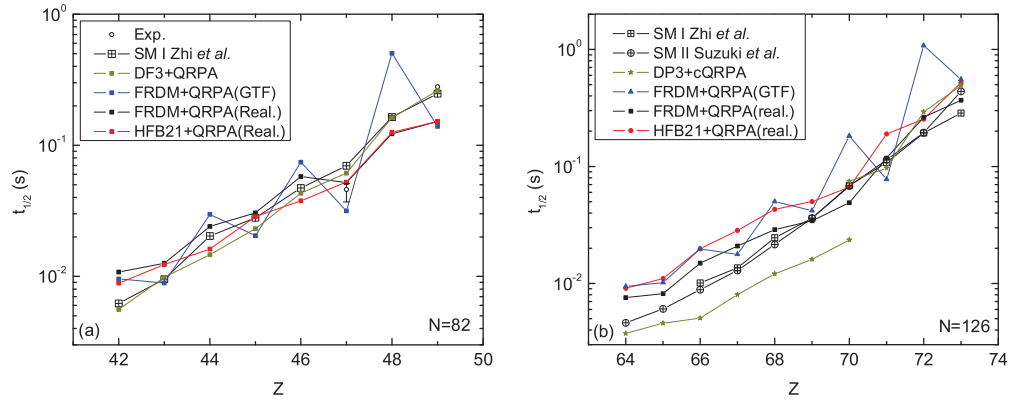

FIG. 1. (Color online) Comparison of half-lives between shell-model calculations (SMI [10], SMII [8], and QRPA calculations) with separable Gamow-Teller forces (GTF) in [12], continuum QRPA in [16,30], and this work for $N = 82$ and $N = 126$ isotonic chains.

IV. RESULTS AND DISCUSSION

With the determined parameters, we proceed to the calculations of isotonic chains on the r-process path in the vicinity of $N = 82$ and $N = 126$. We first show the results with neutron magic numbers $N = 82$ and $N = 126$ where the shell model results for these isotones are available. In Figs. 1–3, we show the comparison of our results with shell-model calculations from Refs. [8,10] (with SMII results [8] updated by correcting a calculations error) and other QRPA calculations such as the QRPA with separable GT force from Ref. [12] and the continuum QRPA from Refs. [16,30]. For the FF part of the decay, Ref. [12] uses the gross theory instead of microscopic calculations, while for all the other calculations, the FF parts are calculated explicitly.

We first compare the most important observables—the half-lives predicted by different methods in Fig. 1. For $N = 82$ isotones, there is good agreement among different methods except those from the separable GT force model of Ref. [12] for which there are systematic overestimations of half-lives on the even-even isotones compared with other methods for the high-Z (low-Q_β) isotones. This is due to their overestimation of the excitation energies and underestimation of the matrix elements due to the lack of particle-particle interactions for the QRPA. This results in odd-even staggering behaviors for the half-lives in separable GT-force calculations. However, when Q_β becomes large, this effect is reduced, as we will see later. Except for Ref. [12], the general discrepancy among different methods for most nuclei is within a factor of 2. This shows a good convergence of the predicted half-lives in microscopic calculations. Compared with the experiments, our method underestimates the half-lives for ^{131}In and ^{130}Cd, especially for the former. The reason for this is that the BCS method does not work well near doubly magic nuclei where the pairing is weak and the BCS solution sometimes overestimates the pairing effect, as we mentioned previously. For ^{130}Cd the reason for the disagreement is due to the energy of the 1^+ state being too low compared to experiment, as seen in Table I. However, we find better agreement for ^{129}Ag, compared with other methods. The results with the FRDM model seem to agree well with the shell-model calculations while those of the HFB21 model give a smoother behavior over the isotonic chains. Compared with the shell-model calculation, we find the trend that when the Q_β value becomes larger, our results give some overestimation of the half-lives.

For the $N = 126$ isotones shown in Fig. 1 the discrepancy among different methods becomes larger. Again, there is a systematic overestimation for results from the separable GT-force model of Ref. [12] for even-even nuclei for larger Z. For the continuum-QRPA method, two sets of results are shown; the results from [16] systematically underestimate the half-lives, while the results from Ref. [30] are closer to other calculations. Recent experimental information on the half-lives of the isotopes with $Z = 75$–79 close to the $N = 126$ r-process waiting-point nuclei [33] are taken into account in Ref. [30]. The two shell-model calculations give similar results for the half-lives. The difference between the two shell-model calculations comes from the different quenching factors and model space adopted, which produce a nearly small constant difference within a factor of about 2. In our calculations, there is a difference of less than a factor of 2 between the two different mass models. When quenching factors with larger quenching are used in the model space of Ref. [8], which is small compared to that in Ref. [10], calculated half-lives come closer to those of Ref. [10] at $Z < 70$. The results with the FRDM model shows a good agreement with the shell-model calculation while those with the HFB21 model give longer half-lives. For most of the nuclei here, with the FRDM model, our results differ from those of the shell model by a factor of less than 2. Overall, we find good agreement for the half-lives for the $N = 126$ isotones among the different methods except those from Ref. [12] at high Z and Ref. [16] at low Z.

Next we compare the results for the β-delayed neutron emission probability P_n in Fig. 2. For the $N = 82$ isotones, unlike the half-life results, there are now larger differences among different methods. There is a general trend that the odd-even nuclei have larger P_n values than their neighboring even-even nuclei, except for results from Ref. [16]. We predict lower P_n values than the other calculations, especially for the even-even nuclei. For ^{130}Cd, our result is smaller than the experimental value of 3.5%. In this case the neutrons come from β decay to the region of excitation in ^{130}In below the β-decay Q_β value of 8.9 MeV and above the neutron decay separation

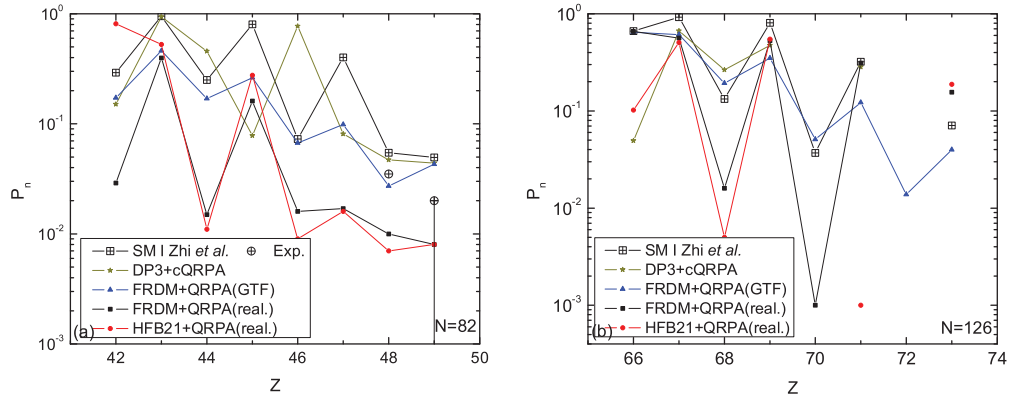

FIG. 2. (Color online) Comparison of total β-delayed neutron emission probability between shell-model calculations [8,10] and QRPA calculations in [12,16,30] and this work for $N = 82$ and $N = 126$ isotonic chains.

energy of 5.1 MeV. Our low P_n value indicates that the QRPA GT distribution in the region of 8 MeV is not spread out enough due to the lack of coupling with particle-hole states. The FRDM + QRPA(GTF) model [12] seems to give better predictions for the P_n values, but this comes from the fact that the energy of the lowest 1^+ state is too high in this case as a much longer half-life is predicted for this nucleus, that is, about four times larger than the experimental half-life.

The same situation occurs for the $N = 126$ isotones (right panel of Fig. 2). The differences among the calculations are quite large for even-even isotones, while there is better agreement for the odd-even cases. In the region $Z < 70$, the P_n values are close to 1. This can be important for r-process evolution. The shell-model calculation [10] predicts larger P_n values than most other calculations for both $N = 82$ and $N = 126$ cases, because, due to the large configuration space in the shell model, the strength is fragmented compared with QRPA calculations and more strength has been distributed above the neutron separation energy threshold.

In order to see the importance of inclusion of the first-forbidden part, we compared the ratios of the FF part to the overall decay width in Fig. 3. For $N = 82$ (except for Ref. [12] in which the FF parts have not been calculated explicitly), the three methods (QRPA, continuum QRPA (cQRPA), and the shell model) predict generally similar ratios. We have lower FF ratios, which are close to those from cQRPA for high Z, and higher FF ratios, which are close to shell-model calculations for low-Z nuclei. On the other hand, this ratio is about the same for the two mass models in our calculation There is a systematic difference between the cQRPA and shell-model calculations and our results are in between. In general, for the $N = 82$ isotonic chain, all the calculations show that the first-forbidden part plays a less important role in β decay. However, this is not the case for the $N = 126$ (right panel of Fig. 3) isotonic chain, where there are large discrepancies among different methods. We obtain FF ratios that decrease with Z, in contrast to the other methods where they increase. Comparing our results carefully with those of Fig. 16 in Ref. [10], we found that the difference comes from the fact that the two methods have different GT strength distributions. Although the excitation energies for 1^+ states are similar (around 2 MeV for both methods for three nuclei ^{194}Er, ^{196}Yb, and ^{198}Hf), the structures of these states are different. In the QRPA calculation, we see a small increase of the energies for the first 1^+ states as the proton number increases, but the energies of the 1^+ states, which give a dominant contribution to the GT decay, however decrease sharply with increasing proton number. This is not seen in shell-model calculations. This means that there may be too much strength present in the low-lying states for $N = 126$ isotones with higher Z due to configuration-space truncations.

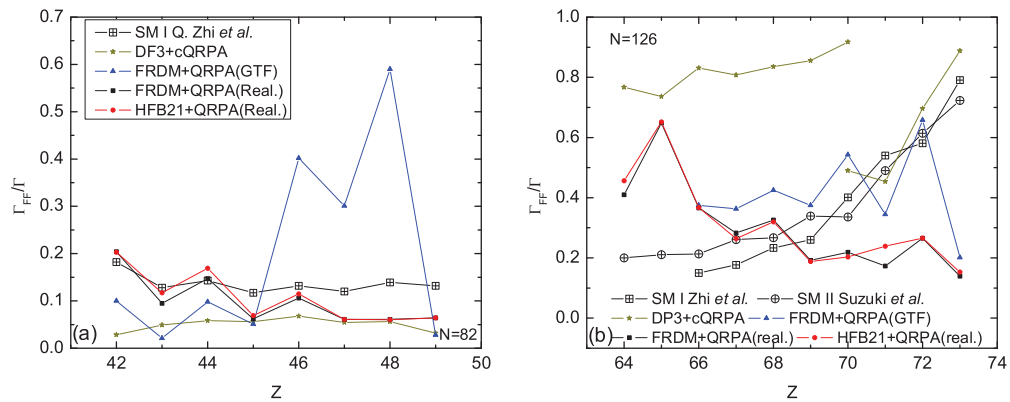

FIG. 3. (Color online) Comparison of ratios of first-forbidden part of the total decay width between shell-model calculations [8,10] and QRPA calculations in [12,16,30] and this work for $N = 82$ and $N = 126$ isotonic chains.

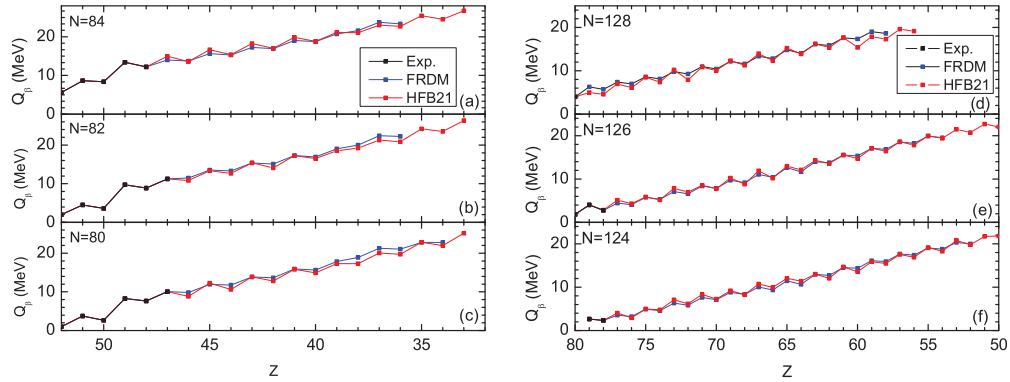

FIG. 4. (Color online) The Q_β values we adopt in our calculation for $N = 80$, 82, and 84 and $N = 124$, 126, and 128 isotones. The meanings of the symbols are explained in the text.

However, shell-model calculations have a too limited model space, which could result in this different behavior of GT strength distributions as well. Although a very large FF ratio was also found in Ref. [16], compared with the same method in Ref. [30], this could be just due to wrongly accounting for parameters in their calculations, and their FF ratios for low-Z isotones may need some updating. On the other hand, we see that, in the two shell-model calculations, the different quenchings and model spaces also give some different ratios as they have similar quenching for the GT part. So, as explained above, the difference between our calculation and the shell-model calculations may came from two aspects, the different configuration space and the different model space, and further investigation is needed to explain the discrepancy for the ratios of FF parts.

The advantage of QRPA methods is that we can calculate with a larger model space more nuclei than those on the magic number line as in the shell-model calculations. Therefore we present more results around the magic number vicinity for even-N nuclei. First, we present the Q_β value sets we use in our calculation in Fig. 4. As mentioned above, we adopt the Q_β values if they are available from experimental measurements as those in [27]. Otherwise, we use two mass models for the sake of comparison: the FRDM [12] model, which is a macroscopic droplet model, and the HFB21 [28] model, which comes from self-consistent microscopic Hartree-Fock-Boglyubov calculations. From Fig. 4, we see that, around neutron number $N = 80$, the Q_β values obtained from the two mass tables are basically the same for most even-even nuclei while there are $\sim$1 MeV differences for most odd-even ones, with generally the FRDM model predicting smaller Q_β values except for those nuclei with lower Z. However, for $N = 82$ and $N = 84$, the FRDM model generally predicts larger Q_β values. For $N = 124$, the same situation occurs as for $N = 82$, with a large difference at low Z. For $N = 126$ and 128, the discrepancy between the two mass models becomes irregular.

We calculated the half-lives of the isotones with the two mass models and the results are presented in Fig. 5. For the $N = 80$, 82, and 84 isotones, we make a comparison with those results in Ref. [12] as well as with some experimental values. When compared with the experimental results, we find very good agreement. In general, the agreement gets better when the nuclei are far from the proton magic number $Z = 50$. The results with $N = 80$ and 84 exhibit the same trends as the $N = 82$ case we analyzed previously. Compared with results obtained in Ref. [12], we would see the same behavior of overestimation of even-even nuclei in their calculation with moderate Q_β values. When the Q_β value increases, the results in both calculations get closer, and, for much larger Q_β values, Ref. [12] predicts shorter half-lives than ours. The reason for this is due to the different treatments of the excitation energies. In Ref. [12], QRPA energies have been used directly

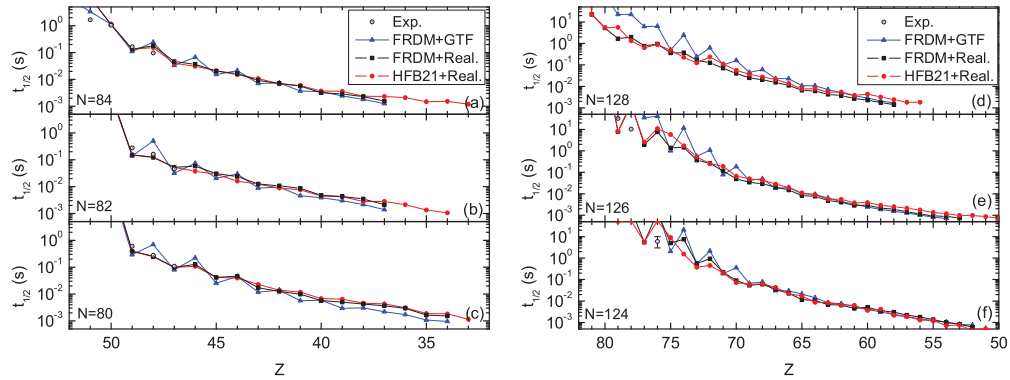

FIG. 5. (Color online) The calculated half-lives from Ref. [12] and our calculations with two mass sets for $N = 80$, 82, and 84 and $N = 124$, 126, and 128 isotones. The comparison between experiments and theories has been presented.

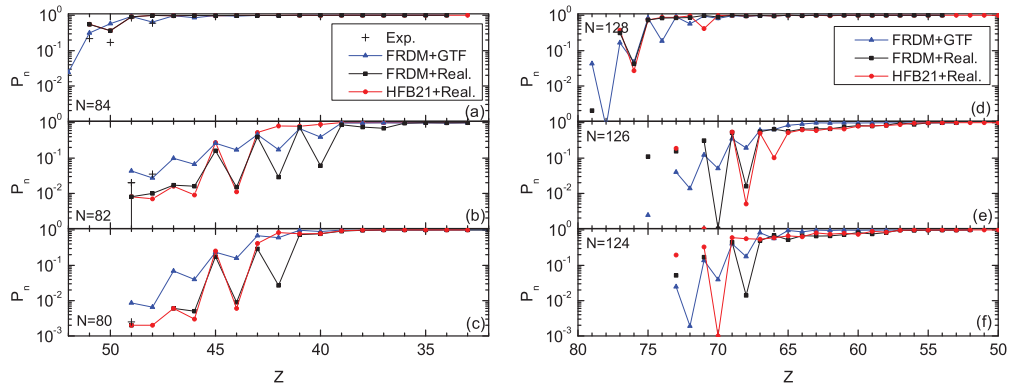

FIG. 6. (Color online) The calculated P_n values from Ref. [12] and our calculations with two mass sets for $N = 80$, 82, and 84 isotones. The comparison between experiments and theories has also been presented.

as the excitation energies, which are in fact about several MeV higher than the actual excitation energies. Although strength spreading has been introduced, even without the quenching effect, the deviation is still large. If Q_β values are large, then the effect from this difference between the QRPA and excitation energies is weakened. Meanwhile, the quenching reduces our decay strength and makes our predicted half-lives longer than theirs. While in the case of odd nuclei, the single-particle transition may play a dominant role for low-lying states, we would not see this large deviation of half-lives for isotones with large proton numbers (Z). Generally, for low Q_β values, deviation occurs for even-even nuclei and agreement is achieved for odd-even nuclei, and for large Q_β values, we have longer half-lives due to the inclusion of quenching. If we compare the results obtained for the two mass models, we see that, for the same nuclei, a large Q_β value shortens the half-life. However, exceptions do exist as the mass model also affects the empirical gap parameters and hence changes the structure indirectly (e.g., in the case of ^{132}Cd, with the same Q_β value, we have a small difference with the two mass sets due to the different gap parameters we obtained). Different mass sets produce different half-lives and their impact on the r-process remains to be investigated. Also, the smoothing behavior of the half-lives on the proton number Z depends on the mass set one chooses. A choice of mass sets may produce an unwanted even-odd staggering behavior. It is somewhat hard to tell whether the staggering comes from the microscopic approaches or the Q_β value sets, due to the uncertainty of the theory. The same conclusion can be drawn for $N = 124$, 126, and 128. One has only limited experimental data in this region, and the agreement for these limited data with the calculations is very poor, as the Q_β values for these nuclei are very small. For $N = 124$ and 126, with increasing Q_β values, our calculation tends to agree with calculations of Ref. [12] for odd-mass nuclei, but for $N = 128$, the deviations always exist. In general, the different mass sets produce a deviation of less than a factor of 2, which is close to the deviations produced from different methods we discussed for the $N = 126$ isotonic chain.

For another measurable, P_n, we have even less experimental data for comparison, see Fig. 6. Our calculation has smaller P_n values compared with experiments, but the deviation is not large especially when P_n is close to 1. For $N = 80$ and 82, the P_n values increase as proton number decreases. For very neutron rich nuclei, the β decay is followed immediately by neutron emission. We see an odd-even staggering behavior, as previously found in shell-model calculations. The deviation between our results and those from Ref. [12] is large in magnitude but keeps the same trends (with the reason for this having been explained above as the strength being shifted to the high-energy region systematically in their calculations). However, the two sets of results seem to agree with each other when $P_n \sim 1$. This is because the neutron separation energies here are pretty smaller; nearly all the strength lies in the window between E_n and Q_β. When one crosses the magic number line $N = 82$, there appear increased P_n values as the nuclei here become less stable against neutron emission, which agrees with the results in Ref. [12]. For the heavier nuclei region with N around 126, the neutron emission probability has not been measured for any nuclei. The general trends here for the two calculations again are the same while they differ in numbers as above. Nuclei beyond the neutron magic number $N = 126$ show large P_n values as for the region of $N \sim 82$.

Due to the drawbacks of the QRPA methods, limited accuracy has been obtained, especially for P_n values. However, one can see some improvements in the QRPA calculations, with the half-lives being closer to the experimental values, and in shell-model calculations compared with results in [12]. For regions where shell-model calculations are absent, decent results have been obtained. To further improve the predicted P_n values, strength spreading from multiphonon effects, such as those from particle-vibration couplings, could be introduced [34,35].

V. CONCLUSION

In this work, we calculated the weak decay properties of even-proton-number isotones near the neutron magic numbers 82 and 126 with the spherical QRPA method with realistic forces. Our results agree well with other calculations on the neutron magic number chains 82 and 126. We gave predictions for more nuclei in this region and compared these with results in Ref. [12]. Different mass models have been used for the

sake of comparison, and they produce a moderate difference for the final results. In general, we made some improvements on the accuracy of decay rates compared with Ref. [12], and their impact on r-process simulations are to be investigated.

ACKNOWLEDGMENT

This work was supported by the U.S. National Science Foundation (Grants No. PHY-0822648 and No. PHY-1068217).

[1] S. E. Woosley, A. Heger, and T. A. Weaver, Rev. Mod. Phys. **74**, 1015 (2002).
[2] J. J. Cowan, F.-K. Thielemann, and J. W. Truran, Phys. Rep. **208**, 267 (1991).
[3] K. Farouqi, K.-L. Kratz, L. I. Mashonkina, B. Pfeiffer, J. J. Cowan, F.-K. Thielemann, and J. W. Truran, Astrophys. J. **694**, L49 (2009).
[4] K. Farouqi, K.-L. Kratz, B. Pfeiffer, T. Rauscher, F.-K. Thilemann, and J. W. Truran, Astrophys. J. **712**, 1359 (2010).
[5] D.-L. Fang, B. A. Brown, and T. Suzuki, arXiv:1211.6070 [nucl-th].
[6] G. Martinez-Pinedo and K. Langanke, Phys. Rev. Lett. **83**, 4502 (1999).
[7] K. Langanke and G. Martinez-Pinedo, Rev. Mod. Phys. **75**, 819 (2003).
[8] T. Suzuki, T. Yoshida, T. Kajino, and T. Otsuka, Phys. Rev. C **85**, 015802 (2012).
[9] J. J. Cuenca-Garcia, G. Martinez-Pinedo, K. Langanke, F. Nowacki, and I. N. Borzov, Eur. Phys. J. A **34**, 99 (2007).
[10] Q. Zhi, E. Caurier, J. J. Cuenca-Garcia, K. Langanke, G. Martinez-Pinedo, and K. Sieja, Phys. Rev. C **87**, 025803 (2013).
[11] P. Moller and J. Randrup, Nucl. Phys. A **514**, 1 (1990).
[12] P. Moller, B. Pfeiffer, and K.-L. Kratz, Phys. Rev. C **67**, 055802 (2003).
[13] H. Homma, E. Bender, M. Hirsch, K. Muto, H. V. Klapdor-Kleingrothaus, and T. Oda, Phys. Rev. C **54**, 2972 (1996).
[14] J. Engel, M. Bender, J. Dobaczewski, W. Nazarewicz, and R. Surman, Phys. Rev. C **60**, 014302 (1999).
[15] I. N. Borzov and S. Goriely, Phys. Rev. C **62**, 035501 (2000).
[16] I. N. Borzov, Phys. Rev. C **67**, 025802 (2003).
[17] J. Suhonen, T. Taigel, and A. Faessler, Nucl. Phys. A **486**, 91 (1988).
[18] O. Civitarese, A. Faessler, and T. Tomoda, Phys. Lett. B **194**, 11 (1987).
[19] H. Behhrens and W. Bühring, *Electron Radial Wave Functions and Nuclear Beta Decay* (Clarendon, Oxford, 1982).
[20] B. A. Brown, Phys. Rev. C **58**, 220 (1998).
[21] R. Machleidt, Adv. Nucl. Phys. **19**, 189 (1989).
[22] B. A. Brown and B. H. Wildenthal, Annu. Rev. Nucl. Part. Sci. **38**, 29 (1988).
[23] G. Martinez-Pinedo, A. Poves, E. Caurier, and A. P. Zuker, Phys. Rev. C **53**, R2602 (1996).
[24] A. Arima, K. Schimizu, W. Bentz, and H. Hyuga, Adv. Nucl. Phys. **18**, 1 (1987).
[25] I. S. Towner, Phys. Rep. **155**, 264 (1987).
[26] G. Audi, A. H. Wapstra, and C. Thibault, Nucl. Phys. A **729**, 337 (2003).
[27] G. Audi, O. Bersillon, J. Blachot, and A. H. Wapstra, Nucl. Phys. A **729**, 3 (2003).
[28] S. Goriely, N. Chamel, and J. M. Pearson, Phys. Rev. Lett. **102**, 152503 (2009).
[29] National Nuclear Data Center, http://www.nndc.bnl.gov/chart/.
[30] I. N. Borzov, Phys. At. Nucl. **74**, 1435 (2011).
[31] I. Dillmann *et al.*, Phys. Rev. Lett. **91**, 162503 (2003).
[32] E. K. Warburton, Phys. Rev. C **44**, 233 (1991).
[33] T. Kurtukian-Nieto *et al.*, Nucl. Phys. A **827**, 587c (2009).
[34] E. Litvinova and P. Ring, Phys. Rev. C **73**, 044328 (2006).
[35] G. Colo, H. Sagawa, and P. F. Bortignon, Phys. Rev. C **82**, 064307 (2010).